Neutron Diffraction Study of the Structures of $Ba_5CuIr_3O_{12}$ and $Ba_{16}Cu_3Ir_{10}O_{39}$

Graeme R. Blake,[†] Peter D. Battle,*[,†] Jeremy Sloan,[†,‡] Jaap F. Vente,[†,||] Jacques Darriet,[§] and François Weill[§]

Inorganic Chemistry Laboratory, University of Oxford, South Parks Road, Oxford OX1 3QR, U.K., Department of Materials, University of Oxford, Parks Road, Oxford OX1 3PH, U.K., and ICMCB, Chateau Brivazac, Av. Dr. Schweitzer, 33608 Pessac Cedex, France

Received December 28, 1998. Revised Manuscript Received March 15, 1999

The crystal structures of $Ba_5CuIr_3O_{12}$ and $Ba_{16}Cu_3Ir_{10}O_{39}$ have been determined using a combination of X-ray and neutron powder diffraction data. Considering their structures to be based on hcp stacks of Ba_3O_9 and Ba_3CuO_6 layers, $Ba_5CuIr_3O_{12}$ has a 10-layer structure, space group $P3c1$ with $a = 10.14055(2)$ Å and $c = 21.65993(9)$ Å. $Ba_{16}Cu_3Ir_{10}O_{39}$ has a 16-layer structure, space group $P321$with $a = 10.13442(2)$ Å and $c = 35.0564(2)$ Å. Sequences of trigonal prismatic and octahedral transition metal sites run in chains parallel to z, with Ba cations located between the chains. The distribution of Ir and Cu cations in the octahedral and trigonal prismatic sites is disordered in both compounds. Cu cations are displaced from the centers of the trigonal prisms toward the rectangular faces. Both materials may also be regarded as commensurate composites of two substructures, sharing common unit cell parameters a and b but with different parameters c_1 and c_2, where the ratio c_1/c_2 is a rational fraction. The relative merits of the oxide layer model and the composite crystal model are discussed.

Introduction

We have recently reported the preparation and structural characterization, by X-ray powder diffraction (XRD) and HRTEM, of the new phases $Ba_5CuIr_3O_{12}$, $Ba_{14}Cu_3Ir_8O_{33}$, $Ba_{16}Cu_3Ir_{10}O_{39}$, and $Ba_9Cu_2Ir_5O_{21}$.[1] We described how these and related structures may be envisaged as hcp stacks (*aba*) of two different types of pseudo-close-packed layers with the stoichiometries A_3O_9 and $A_3A'O_6$ (Figure 1). The $A_3A'O_6$ layer is derived from the A_3O_9 layer by the systematic replacement of three oxygen atoms by an A′ atom. In our compounds A = Ba and A′ = Cu, and Ir occupies the octahedral interstices between adjacent layers. In an alternative but equivalent view, each of these structures may be described in a trigonal or rhombohedral unit cell with three crystallographically distinct chains of cation-containing polyhedra running parallel to the z axis. All three chains contain the same sequence of IrO_6 octahedra and CuO_6 prisms, but there is an offset between neighboring chains. The Ba atoms occupy coordination sites between the chains. In a number of related cases, for example $Ba_6ZnIr_4O_{15}$ and $Ba_4CuIr_2O_9$,[2,3] this description of the structures has proved to be inadequate.

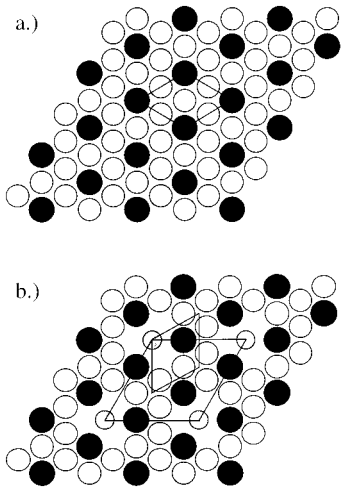

Figure 1. (a) A_3O_9 layer and (b) A_3O_6 layer, with trigonal prismatic sites (A′) marked by lightly shaded circles. The two-dimensional unit cells of both layer types are shown, with $a' = \sqrt{3}a$.

XRD and electron diffraction (ED) studies have shown these compounds to be incommensurate along [001]. Their structures can be described as composites containing two substructures, with the same unit cell parameters a and b but with different parameters c_1 and c_2; c_1 is associated with the columns of Ba cations, and is the mean separation of equivalent, (i.e., alternate) pseudo-close-packed planes in the *aba* hcp stack, whereas c_2 is the mean spacing of the cations within the poly-

* To whom correspondence should be addressed.
[†] Inorganic Chemistry Laboratory, University of Oxford.
[‡] Department of Materials, University of Oxford.
[§] ICMCB.
[||] Present address: Cinvestav-IPN Unidad Merida, Departemento de Fisica Aplicada, Carretera Ant. a Progreso km 6, Apartado Postal #73 Cordemex, Merida, Yucatan, 97310, Mexico.

(1) Blake, G. R.; Sloan, J.; Vente, J. F.; Battle, P. D. *Chem. Mater.* **1998**, *10*, 3536.
(2) Battle, P. D.; Blake, G. R.; Darriet, J.; Gore J. G.; Weill, F. *J. Mater. Chem.* **1997**, *7*, 1559.
(3) Battle, P. D.; Blake, G. R.; Sloan, J.; Vente, J. F. *J. Solid State Chem.* **1998**, *136*, 103.

10.1021/cm9807844 CCC: $18.00
Published on Web 05/15/1999

hedral chains. The unit cell is commensurate when $pc_1 = qc_2$, that is $c_1/c_2 = q/p$ (p and q are integers), and incommensurate when c_1/c_2 is not a rational fraction. The phases $Ba_5CuIr_3O_{12}$, $Ba_{14}Cu_3Ir_8O_{33}$, $Ba_{16}Cu_3Ir_{10}O_{39}$, and $Ba_9Cu_2Ir_5O_{21}$ are commensurate and have c_1/c_2 ratios of 8/5, 11/7, 13/8, and 14/9, respectively. However, each of these phases has at least two possible structures because the relative translations of adjacent transition metal chains may vary. As a result of our previous study by XRD and ED, we were able to rule out some candidate structures, but we were unable to determine the structure of each composition uniquely because of the inadequate definition of the anion sublattice. We describe below a continuation of our structural investigations of these materials using neutron diffraction (ND) data, our aim being to locate the oxide ions more accurately and hence to be able to distinguish between the different candidate structures for each stoichiometry. The relative merits of the layer-structure model and the composite-crystal model are discussed in the light of our results.

Experimental Section

Polycrystalline samples (5 g) of nominal compositions $Ba_5CuIr_3O_{12}$ and $Ba_{16}Cu_3Ir_{10}O_{39}$ were prepared using standard solid-state synthesis methods. We were unable to prepare commensurate samples of $Ba_{14}Cu_3Ir_8O_{33}$ and $Ba_9Cu_2Ir_5O_{21}$ large enough to be used in neutron diffraction experiments. Stoichiometric, pelletized mixtures of the starting materials $BaCO_3$, CuO, and Ir contained in alumina crucibles were heated in air, initially overnight at 800 °C and subsequently at the following temperatures: $Ba_5CuIr_3O_{12}$, 1200 °C (4 h), 1250 °C (24 h); $Ba_{16}Cu_3Ir_{10}O_{39}$, 1220 °C (2 h), 1250 °C (1 h), 1275 °C (3 h), 1300 °C (3 h). The progress of the reactions was followed by XRD, and they were deemed to be complete when the measured diffraction pattern could be accounted for by the presence of one commensurate phase having trigonal symmetry. The XRD data were collected at room temperature over the angular range $10° \leq 2\theta$ (deg) $\leq 110°$, with a step size of $\Delta 2\theta = 0.02°$, on a Siemens D5000 diffractometer operating with Cu $K\alpha_1$ radiation in Bragg−Brentano geometry. Time-of-flight neutron diffraction data were obtained on the instrument HRPD at the ISIS facility, Rutherford Appleton Laboratory. Data were collected at room temperature in the d-spacing range $0.64 \leq d$ (Å) ≤ 2.5, on samples of mass ~4 g contained in cylindrical vanadium cans. An initial absorption correction was applied to the data at this stage, the absorption cross-section of iridium being high. The absorption correction program SCORR, incorporated in the Genie spectrum manipulation software,[4] was used. The data were analyzed by the Rietveld method,[5] as implemented in the GSAS program suite.[6] The background levels of both the XRD and ND profiles were modeled using Chebyschev polynomials of the first kind (12 and 10 parameters, respectively). The peak shape of the XRD profiles was described by a pseudo-Voigt function (eight parameters) and that of the ND profiles by a convolution of back-to-back exponentials and a pseudo-Voigt function (six parameters). A wavelength-dependent absorption correction according to an empirical formula after Hewat[7] was included for the ND data.

Results

The ND and XRD patterns of our final products were consistent with each other and with the data collected on our previous samples.[1] As discussed previously, different stacking sequences of oxide layers are possible for each of the materials prepared above. Rietveld refinements, initially using only ND data, were carried out on each candidate structure.

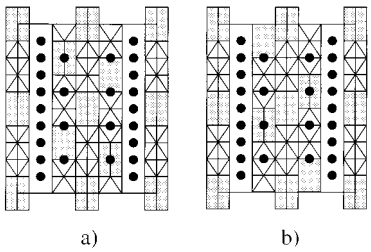

Figure 2. Idealized structures of the 10-layer compound $Ba_5CuIr_3O_{12}$ (models **a** and **b**), viewed along [110]. Trigonal prisms are shaded, octahedra are unshaded, and black circles represent Ba.

The two possible structures for the phase of composition $Ba_5CuIr_3O_{12}$ are shown in Figure 2; model **b** is derived from model **a** by translating the transition metal chains centered on (1/3, 2/3, z) and (2/3, 1/3, z) a distance of $c/10$ parallel to the c direction with respect to the chain at (0, 0, z), the translations of the former two chains being in opposite directions. Our previously reported XRD study suggested that model **a** was the correct one, and we assigned the space group $P321$ to the structure. This choice, which excludes the presence of a c glide plane, was based on the observation of $00l$, $l = 2n + 1$ reflections in the $[1\bar{1}0]$ zone ED pattern of our sample. However, these reflections were not observed in the [010] zone, consistent with their being an artifact produced by double diffraction effects. If we assume this to be the case, our XRD and ED data can be indexed in space group $P3c1$ or $P\bar{3}c1$. We analyzed our neutron data in both of these space groups and obtained significantly better agreement in noncentrosymmetric $P3c1$, although the principal structural features described below were insensitive to the choice of space group. In the refinement of model **a**, the Ir^{4+} cations were initially assigned to the octahedral sites and the Cu^{2+} cations to the trigonal prismatic sites. However, a difference Fourier map suggested that the Cu^{2+} cations were displaced from the 3-fold axis which runs along the center of the cation chains, toward the rectangular faces of the trigonal prisms. The introduction of such a displacement resulted in an improvement in the agreement between the observed and calculated diffraction profiles. A further improvement was achieved when the distribution of Cu^{2+} and Ir^{4+} over the six-coordinate sites was refined. The best fit was obtained by setting the occupancy of the central octahedra of the trimers to 100% iridium, but with the Ir/Cu ratio in the other polyhedra allowed to vary. A difference Fourier map suggested that although the Cu^{2+} cations in the prisms lie near the rectangular faces, the prismatic Ir^{4+} cations lie on the 3-fold axis. The isotropic temperature factors of the displaced Cu cations in the trigonal prismatic sites were set to zero to avoid meaningless negative values, and a single value was used for the temperature factor of trigonal prismatic Ir. Although the essential features of the model were derived from the ND data, the refinement was stabilized and the standard deviations of the atomic parameters were ultimately minimized by the simultaneous analysis of

(4) David, W. I. F.; Johnson, M. W.; Knowles, K. J.; Moreton-Smith, C. M.; Crosbie, G. D. ; Campbell, E. P.; Graham, S. P.; Lyall, J. S. *Rutherford-Appleton Laboratory Report* RAL-87-010, 1987.

(5) Rietveld, H. M. *J. Appl. Crystallogr.* **1969**, *2*, 65.

(6) Larson, A. C.; von Dreele, R. B. *General Structure Analysis System (GSAS)*; Report LAUR 86-748, Los Alamos National Laboratories: Los Alamos, NM, 1990.

(7) Hewat, A. W. *Acta Crystallogr.* **1979**, *A35*, 248.

Table 1. Atomic Parameters for $Ba_5CuIr_3O_{12}$ (Model a)

atom	site	fractional occupancy[a]	x	y	z	U_{iso}, Å^2	atom	site	fractional occupancy[a]	x	y	z	U_{iso}, Å^2
Ba1	6d		0.000(3)	0.354(2)	0.016(1)	0.009(3)	Cu10	6d	0.212(4)	0.927(3)	0	0.015(2)	0
Ba2	6d		0.321(2)	0.333(3)	0.112(1)	0.008(3)	Cu11	6d	0.212(4)	0.396(4)	2/3	0.312(2)	0
Ba3	6d		0.997(2)	0.326(2)	0.209(1)	0.013(3)	Cu12	6d	0.212(4)	0.613(4)	1/3	0.219(2)	0
Ba4	6d		0.333(2)	0.320(2)	0.311(1)	0.012(4)	O1	6d		0.326(3)	0.502(2)	0.005(1)	0.009(4)
Ba5	6d		0.996(3)	0.337(3)	0.413(1)	0.021(4)	O2	6d		0.672(3)	0.180(2)	0.031(1)	0.012(4)
Ir1/Cu1	2a	0.818(6)	0	0	0.146(1)	0.005(4)	O3	6d		0.997(3)	0.146(3)	0.087(1)	0.022(5)
Ir2/Cu2	2a	1.0	0	0	0.267(1)	0.007(3)	O4	6d		0.340(3)	0.825(2)	0.122(1)	0.006(4)
Ir3/Cu3	2a	0.818(6)	0	0	0.390(1)	0.034(6)	O5	6d		0.817(3)	0.335(3)	0.147(2)	0.030(6)
Ir4/Cu4	2b	1.0	1/3	2/3	0.061(1)	0.004(3)	O6	6d		0.842(3)	0.002(3)	0.211(1)	0.010(4)
Ir5/Cu5	2b	0.818(6)	1/3	2/3	0.178(1)	0.008(4)	O7	6d		0.331(4)	0.510(3)	0.237(1)	0.013(4)
Ir6/Cu6	2b	0.818(6)	1/3	2/3	0.439(1)	0.021(5)	O8	6d		0.002(3)	0.157(3)	0.326(1)	0.005(4)
Ir7/Cu7	2c	0.818(6)	2/3	1/3	0.092(1)	0.045(7)	O9	6d		0.826(3)	0.335(4)	0.299(2)	0.021(5)
Ir8/Cu8	2c	0.818(6)	2/3	1/3	0.349(1)	0.000(3)	O10	6d		0.852(2)	0.998(3)	0.445(1)	0.009(4)
Ir9/Cu9	2c	1.0	2/3	1/3	0.473(1)	0.014(5)	O11	6d		0.331(2)	0.497(2)	0.398(1)	0.016(3)
Ir10	2a	0.364(12)	0	0	0.028(2)	0.008(4)	O12	6d		0.665(3)	0.177(2)	0.412(1)	0.009(5)
Ir11	2b	0.364(12)	1/3	2/3	0.297(2)	0.008(4)							
Ir12	2c	0.364(12)	2/3	1/3	0.241(2)	0.008(4)							

[a] Tabulated values for Ir1/Cu1 to Ir9/Cu9 are fractional occupancies of Ir; Ir fraction + Cu fraction = 1. For trigonal prismatic atoms Ir10 to Ir12 and Cu10 to Cu12, (3 × Cu fraction) + Ir fraction = 1. Space group $P3c1$; $a = 10.14055(2)$ Å, $c = 21.65993(9)$ Å, $V = 1928.903(8)$ Å^3; Values of U_{iso} for Cu10 to Cu12 were fixed at zero. Neutron data: Rwp = 5.89%, Rp = 5.25%. X-ray data: Rwp = 13.68%, Rp = 10.34%. Combined data: Rwp = 7.04%, Rp = 9.71%, $\chi^2 = 2.174$.

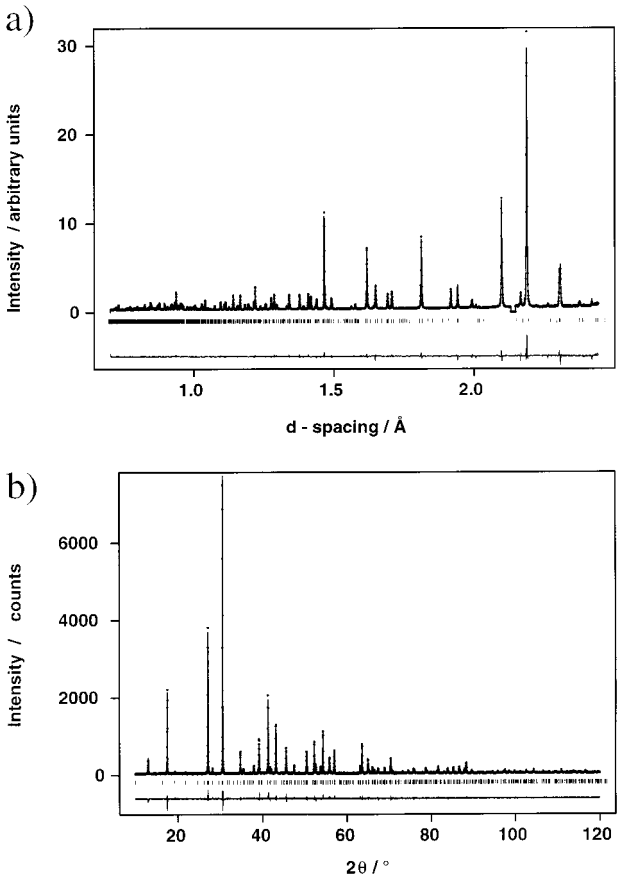

Figure 3. Observed, calculated and difference (a) neutron and (b) X-ray diffraction profiles of $Ba_5CuIr_3O_{12}$ (model **a**). Reflection positions are marked.

XRD and ND data sets. The refinement then converged smoothly with Rwpr = 7.04% and $\chi^2 = 2.174$ for the combined data sets. Refinements in the centrosymmetric space group $P\bar{3}c1$ resulted in Rwpr = 7.99% and $\chi^2 = 2.724$. The diffraction profiles are shown in Figure 3, the refined structural parameters are given in Table 1 and a list of selected bond distances is presented in Table 2. A refinement of model **b** in space group $P3c1$ was also attempted using combined XRD and ND data sets. The same types of disorder as for model **a** were introduced but the fit of the observed to calculated diffraction profiles was worse (Rwpr = 7.63% and $\chi^2 = 2.540$). Furthermore, one of the iridium−oxygen bond distances was unreasonably short, at 1.77(4) Å. Model **b** may therefore be discounted. A [110] view of the refined structure of model **a** is shown in Figure 4a. In Figure 4b only the oxygen and barium positions are shown. Figure 5a shows the coordination environment of Cu and Ir in the chain centered on (0, 0, z). In Figure 5b the trigonal prism containing Cu10 and Ir10 is shown, looking along [001].

The phase with composition $Ba_{16}Cu_3Ir_{10}O_{39}$ has four possible structures, all with 16 layers and trigonal symmetry, shown in Figure 6. The translation of the chain centered on (1/3, 2/3, z) relative to that centered on (0, 0, z) may be 7c/16 (model **a**), c/4 (model **b**), c/8 (model **c**), or c/16 (model **d**). In our previously reported XRD study there was little to choose among models **a**, **b,** and **c**, although model **d** was ruled out. In the ND study described below, refinements were again carried out on all four candidate structures. The space group with highest symmetry that may be assigned is $P321$; unlike the case of $Ba_5CuIr_3O_{12}$ there is no ambiguity, and the structures cannot be described in $P3c1$ or $P\bar{3}c1$. In similar fashion to the case of $Ba_5CuIr_3O_{12}$, two types of disorder were introduced. The Cu^{2+} ions were allowed to move toward the rectangular faces of the trigonal prisms and the distribution of Ir^{4+} and Cu^{2+} over the octahedra and trigonal prisms was refined. The occupation of the central octahedra in the trimers and tetramers was set to 100% Ir and the Ir cations in the trigonal prisms were constrained to lie on the 3-fold axis. This distribution of cations was suggested both by difference Fourier maps and by the quality of the fit of observed to calculated diffraction profiles. When only ND data were utilized, the refinement diverged due to the large number of atomic parameters involved, and a simultaneous analysis of XRD and ND data sets was necessary. However, simultaneous refinement of all the oxygen and barium atomic positions was still not possible and constraints were therefore introduced. It was observed that the x and y coordinates of most oxygen and barium atoms were strongly correlated. Therefore, in prelimi-

Table 2. Selected Bond Lengths (Å) for $Ba_5CuIr_3O_{12}$ (Model a)

Ir1−Ir2	2.62(2)	Ir6−Ir11	3.09(4)	Ir3−O8	2.10(2) ×3	Ir8−O9	1.94(2) ×3
Ir1−Cu10	2.93(5) ×3	Ir7−Ir9	2.58(3)	Ir3−O10	1.91(2) ×3	Ir8−O12	2.09(2) ×3
Ir1−Ir10	2.56(4)	Ir7−Cu12	2.81(4) ×3	Ir4−O1	2.03(2) ×3	Ir9−O2	2.03(2) ×3
Ir2−Ir3	2.67(3)	Ir7−Ir12	3.24(5)	Ir4−O4	2.05(2) ×3	Ir9−O12	2.06(2) ×3
Ir3−Cu10	2.81(5) ×3	Ir8−Ir9	2.69(2)	Ir5−O4	2.00(2) ×3	Ir10−O3	1.97(3) ×3
Ir3−Ir10	2.98(4)	Ir8−Cu12	2.86(4) ×3	Ir5−O7	2.01(2) ×3	Ir10−O10	2.34(3) ×3
Ir4−Ir5	2.55(2)	Ir8−Ir12	2.33(4)	Ir6−O1	2.17(2) ×3	Ir11−O7	2.04(3) ×3
Ir4−Ir6	2.63(3)	Ir1−O3	1.97(2) ×3	Ir6−O11	1.94(2) ×3	Ir11−O11	2.78(3) ×3
Ir5−Cu11	2.96(4) ×3	Ir1−O6	2.14(2) ×3	Ir7−O2	2.06(3) ×3	Ir12−O5	2.55(4) ×3
Ir5−Ir11	2.56(4)	Ir2−O6	2.02(2) ×3	Ir7−O5	1.93(3) ×3	Ir12−O9	2.03(3) ×3
Ir6−Cu11	2.83(4) ×3	Ir2−O8	2.04(2) ×3				
Cu10−O3	2.02(4)	Cu10−O10	2.00(4)	Cu11−O11	2.38(3)	Cu12−O5	2.59(4)
Cu10−O3	2.04(4)	Cu11−O7	2.14(4)	Cu11−O11	2.99(4)	Cu12−O9	2.22(4)
Cu10−O3	2.73(4)	Cu11−O7	2.13(3)	Cu12−O5	2.06(4)	Cu12−O9	2.23(4)
Cu10−O10	2.71(4)	Cu11−O7	2.74(4)	Cu12−O5	2.06(4)	Cu12−O9	2.75(4)
Cu10−O10	2.01(4)	Cu11−O11	2.39(3)				
Ba1−O1	2.88(4)	Ba2−O3	2.91(3)	Ba3−O6	2.91(3)	Ba4−O11	2.60(2)
Ba1−O1	2.82(3)	Ba2−O3	2.95(3)	Ba3−O7	2.99(4)	Ba4−O12	2.79(3)
Ba1−O2	2.90(4)	Ba2−O4	2.90(3)	Ba3−O7	3.07(4)	Ba5−O1	2.65(3)
Ba1−O2	2.82(4)	Ba2−O4	2.88(4)	Ba3−O8	3.07(2)	Ba5−O2	3.10(3)
Ba1−O3	2.60(3)	Ba2−O5	3.12(3)	Ba3−O9	2.63(3)	Ba5−O8	2.65(3)
Ba1−O4	2.85(3)	Ba2−O5	3.14(3)	Ba4−O6	2.76(3)	Ba5−O9	3.02(3)
Ba1−O5	3.33(3)	Ba2−O6	2.73(2)	Ba4−O7	2.53(3)	Ba5−O10	3.06(4)
Ba1−O10	2.60(3)	Ba2−O7	3.22(3)	Ba4−O8	2.93(4)	Ba5−O10	3.06(4)
Ba1−O11	3.02(2)	Ba3−O3	3.21(3)	Ba4−O8	2.85(3)	Ba5−O11	2.96(3)
Ba1−O12	2.83(3)	Ba3−O4	2.66(2)	Ba4−O9	2.93(4)	Ba5−O11	2.94(3)
Ba2−O1	2.87(3)	Ba3−O5	2.31(3)	Ba4−O9	2.84(4)	Ba5−O12	2.91(3)
Ba2−O2	2.60(3)	Ba3−O6	2.84(3)	Ba4−O10	3.41(3)	Ba5−O12	2.85(4)

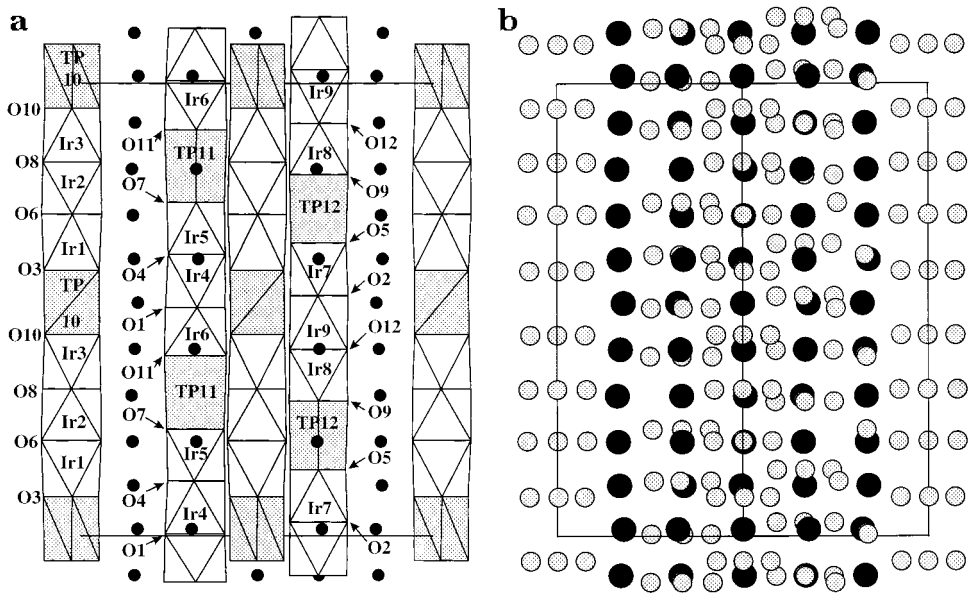

Figure 4. (a) Refined structure of $Ba_5CuIr_3O_{12}$ (model **a**) viewed along [110]; trigonal prisms are shaded, octahedra are unshaded, and black circles represent Ba. Trigonal prisms are numbered after the Ir and Cu atoms they contain. (b) A view of the Ba/O atomic arrangement along [110]. Black circles represent Ba; lightly shaded circles represent O.

nary refinements, the shifts of the Ba *x* and *y* coordinates were set to be equal. In addition, either the *x* or the *y* coordinate of each oxygen was fixed to its ideal value, preventing the rotation of triangles of oxide ions around the 3-fold axis. Oxide ions were thus only allowed to move along [100], [010], and [110] in the (*xy*) plane, but free movement in the *z* direction was allowed. Convergence was then achieved. In subsequent refinements the strict constraints on the atomic coordinates were removed and replaced by soft constraints on the Ir−O and Ba−O bond lengths. These distances were constrained to the values determined in the preliminary refinement, with an allowed standard deviation of 0.05 Å. The weighting factor for the soft constraints was reduced to the minimum value possible for convergence (FACTR = 0.5), giving the Ba and O coordinates the maximum possible freedom. The large number of parameters also led to a reduction in the number of isotropic temperature factors that could be used; five were assigned: one each for Ba, O, octahedral Ir/Cu, trigonal prismatic Cu, and trigonal prismatic Ir. In all cases the isotropic temperature factor of Cu in the trigonal prismatic sites was set to zero since it refined to a negative value. Of the four candidate structures, the best fit was given by model **c** (Rwpr = 7.31%, χ^2 = 2.556). Some of the refined bond distances, however, are very short; for example an Ir9−O12 distance of 1.84(3) Å. Models **a** and **b** were not stable when the Ba and O atoms were allowed to move freely, although model **a** gave a similar fit to model **c** after the preliminary stage.

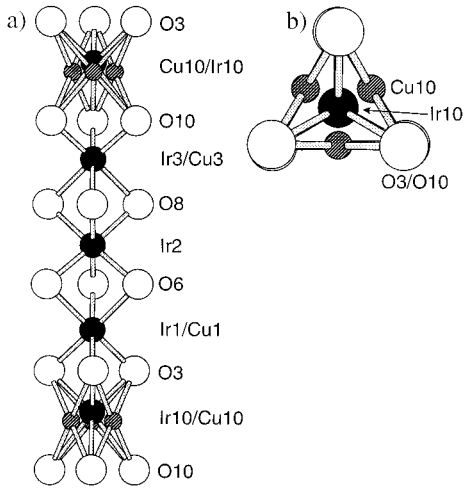

Figure 5. (a) Local coordination around Ir and Cu cations in $Ba_5CuIr_3O_{12}$ (model **a**). Dark circles represent Ir, lightly shaded circles represent Cu, and open circles represent O. (b) [001] view of a trigonal prism. Dark circle represents Ir, lightly shaded circles represent Cu, and open circles represent O.

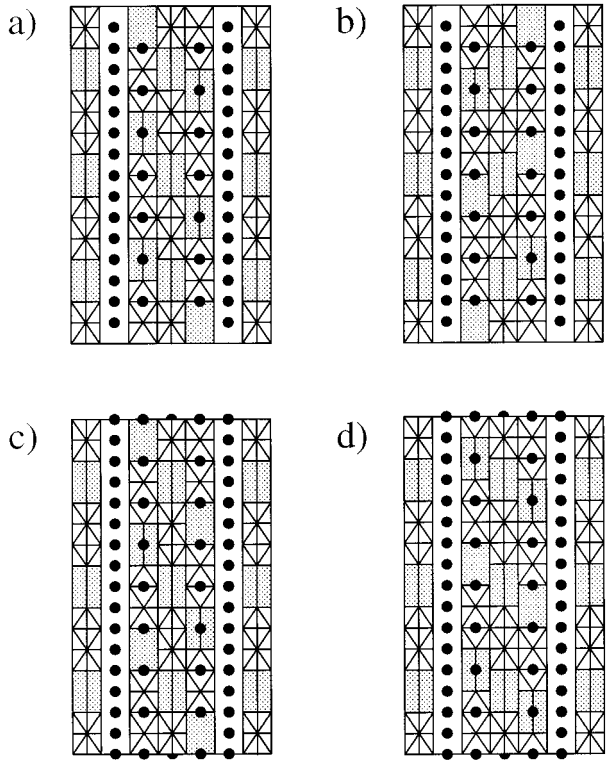

Figure 6. Idealized structures of the 16-layer compound $Ba_{16}Cu_3Ir_{10}O_{39}$ (models **a**, **b, c,** and **d**). Trigonal prisms are shaded, octahedra are unshaded, and black circles represent Ba.

Model **d**, as expected from our previous study, gave a worse fit (Rwpr = 8.04%, χ^2 = 3.136) and may be discounted. The diffraction profiles for model **c** are shown in Figure 7, the refined structural parameters are given in Table 3 and a list of selected bond distances is presented in Table 4. The refined structure of model **c**, viewed along [110], is shown in Figure 8a. In Figure 8b, only the oxygen and barium positions are shown.

Discussion

It was relatively straightforward to discern the correct stacking sequence of oxide layers for the 10-layer phase $Ba_5CuIr_3O_{12}$, the refinement of model **a** giving a significantly better fit than that of model **b**. The refined structure of model **a** contains a large variation of cation−cation distances within the chains; Ir−Ir distances range from 2.33(4) Å for Ir8−Ir12 to 3.24(5) Å for Ir7−Ir12. The longest and shortest distances occur where Ir cations are displaced from the centers of trigonal prisms toward one of the triangular faces. Many of the Ir−O distances in the octahedral sites are much shorter than expected for Ir^{4+}, as low as 1.91(2) Å for Ir3−O10; a typical Ir^{4+}−O bond distance is 2.05 Å.[8] However, as these short distances are due to the displacement of Ir from the center of the octahedra, parallel to *c*, in every case they are compensated for by longer than expected distances to the oxide ions on the opposite faces of the octahedra. The average value of the Ir−O distances over all the octahedral sites is 2.03 Å, which is typical for Ir^{4+}. There is substantial disorder in the distribution of Ir and Cu cations over the octahedral and trigonal prismatic sites; the occupancy of Ir in the outer octahedra of the trimers refined to 81.8(6)%, which is close to the value (78.8(7)%) determined previously in our XRD study of a different sample of the same material. The precise arrangement of atoms within the trigonal prismatic sites is somewhat unclear. Difference Fourier maps showed that some atoms are located toward the rectangular faces while others

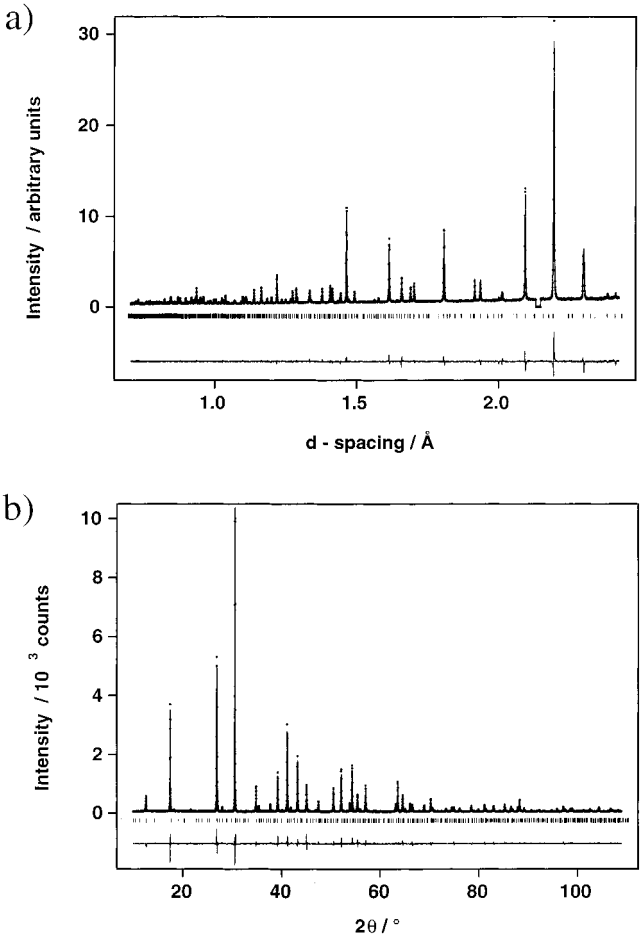

Figure 7. Observed, calculated, and difference (a) neutron and (b) X-ray diffraction profiles of $Ba_{16}Cu_3Ir_{10}O_{39}$ (model **a**). Reflection positions are marked.

(8) Powell, A. V.; Battle, P. D.; Gore, J. G. *Acta Crystallogr.* **1993**, *C49*, 852.

Table 3. Atomic Parameters for $Ba_{16}Cu_3Ir_{10}O_{39}$ (Model c)

atom	site	fractional occupancy[a]	*x*	*y*	*z*	U_{iso}, Å^2	atom	site	fractional occupancy[a]	*x*	*y*	*z*	U_{iso}, Å^2
Ba1	3e		0	0.325(4)	0	0.0147(6)	Cu16	6g	0.182(5)	0.06(1)	0	0.189(3)	0
Ba2	6g		0.326(4)	0.331(4)	0.0612(7)	0.0147(6)	Cu17	3f	0.182(5)	0.95(2)	0	0.5	0
Ba3	6g		0.012(3)	0.338(3)	0.1290(5)	0.0147(6)	Cu18	6g	0.182(5)	0.40(1)	2/3	0.317(3)	0
Ba4	6g		0.350(3)	0.351(3)	0.1870(7)	0.0147(6)	Cu19	6g	0.182(5)	0.28(1)	2/3	0.624(3)	0
Ba5	6g		0.983(3)	0.317(3)	0.2464(6)	0.0147(6)	Cu20	6g	0.182(5)	0.41(1)	2/3	0.937(3)	0
Ba6	6g		0.328(4)	0.325(4)	0.3123(7)	0.0147(6)	O1	3e		0.844(4)	0	0	0.0136(5)
Ba7	6g		0.017(3)	0.335(4)	0.3736(5)	0.0147(6)	O2	6g		0.666(4)	0.189(3)	0.0211(8)	0.0136(5)
Ba8	6g		0.341(4)	0.343(3)	0.4338(6)	0.0147(6)	O3	6g		0.997(4)	0.157(4)	0.0714(8)	0.0136(5)
Ba9	3f		0	0.343(4)	0.5	0.0147(6)	O4	6g		0.333(5)	0.825(4)	0.0558(8)	0.0136(5)
Ir1/Cu1	2c	1.0	0	0	0.0364(8)	0.0135(5)	O5	6g		0.854(3)	0.000(4)	0.1463(8)	0.0136(5)
Ir2/Cu2	2c	0.773(8)	0	0	0.1147(7)	0.0135(5)	O6	6g		0.669(5)	0.176(4)	0.1126(8)	0.0136(5)
Ir3/Cu3	2c	0.773(8)	0	0	0.2712(8)	0.0135(5)	O7	6g		0.335(5)	0.510(4)	0.1264(8)	0.0136(5)
Ir4/Cu4	2c	1.0	0	0	0.3459(7)	0.0135(5)	O8	6g		0.334(4)	0.824(4)	0.1988(8)	0.0136(5)
Ir5/Cu5	2c	0.773(8)	0	0	0.4175(8)	0.0135(5)	O9	6g		0.821(4)	0.331(6)	0.1823(8)	0.0136(5)
Ir6/Cu6	2d	0.773(8)	1/3	2/3	0.0164(8)	0.0135(5)	O10	6g		0.840(4)	0.996(4)	0.2376(9)	0.0136(5)
Ir7/Cu7	2d	1.0	1/3	2/3	0.0917(8)	0.0135(5)	O11	6g		0.664(5)	0.176(3)	0.2589(7)	0.0136(5)
Ir8/Cu8	2d	0.773(8)	1/3	2/3	0.1628(8)	0.0135(5)	O12	6g		0.328(4)	0.501(3)	0.2640(7)	0.0136(5)
Ir9/Cu9	2d	0.773(8)	1/3	2/3	0.2410(9)	0.0135(5)	O13	6g		0.000(5)	0.157(4)	0.3095(9)	0.0136(5)
Ir10/Cu10	2d	1.0	1/3	2/3	0.3988(8)	0.0135(5)	O14	6g		0.811(4)	0.336(5)	0.3285(8)	0.0136(5)
Ir11/Cu11	2d	1.0	1/3	2/3	0.4728(7)	0.0135(5)	O15	6g		0.843(4)	0.004(4)	0.3816(9)	0.0136(5)
Ir12/Cu12	2d	0.773(8)	1/3	2/3	0.5460(8)	0.0135(5)	O16	6g		0.342(4)	0.514(3)	0.3605(8)	0.0136(5)
Ir13/Cu13	2d	0.773(8)	1/3	2/3	0.7094(8)	0.0135(5)	O17	6g		0.005(4)	0.170(3)	0.4476(7)	0.0136(5)
Ir14/Cu14	2d	1.0	1/3	2/3	0.7813(8)	0.0135(5)	O18	6g		0.817(4)	0.333(5)	0.4196(8)	0.0136(5)
Ir15/Cu15	2d	0.773(8)	1/3	2/3	0.8562(8)	0.0135(5)	O19	6g		0.333(5)	0.823(4)	0.4363(8)	0.0136(5)
Ir16	2c	0.45(2)	0	0	0.199(2)	0.014(4)	O20	6g		0.333(4)	0.506(3)	0.5075(8)	0.0136(5)
Ir17	2c	0.227(8)	0	0	0.492(4)	0.014(4)							
Ir18	2d	0.45(2)	1/3	2/3	0.329(2)	0.014(4)							
Ir19	2d	0.45(2)	1/3	2/3	0.637(2)	0.014(4)							
Ir20	2d	0.45(2)	1/3	2/3	0.928(2)	0.014(4)							

[a] Tabulated values for Ir1/Cu1 to Ir15/Cu15 are fractional occupancies of Ir; Ir fraction + Cu fraction = 1. For trigonal prismatic atoms Ir16,18,19,20 and Cu16,18,19,20, (3 × Cu fraction) + Ir fraction = 1. For trigonal prismatic atoms Ir17 and Cu17, (3 × Cu fraction) + (2 × Ir fraction) = 1. Space group *P*321; $a = 10.13442(2)$ Å, $c = 35.0564(2)$ Å, $V = 3118.24(2)$ Å^3; values of U_{iso} for Cu16 to Cu20 were fixed at zero. Neutron data: *R*wp = 6.17%, *R*p = 5.43% X-ray data: *R*wp = 12.64%, *R*p = 9.70% Combined data: *R*wp = 7.30%, *R*p = 9.23%, $\chi^2 = 2.551$

remain on the 3-fold axis, displaced up or down, parallel to *c*, from the center of the trigonal prism. The best fit was obtained on allowing Cu^{2+} to be displaced toward the rectangular faces, leaving Ir^{4+} to occupy the positions on the 3-fold axis, which is unsurprising given the disposition of Cu^{2+} toward square-planar coordination. A similar displacement of Cu^{2+} has been seen in the structurally related compounds $Sr_4CuIr_2O_9$,[3] Sr_3CuIrO_6,[9] Sr_3CuPtO_6,[10] and $Ca_{3.5}Cu_{0.5}PtO_6$.[11] Figure 5b shows an example of the resulting cation distribution. However, the standard deviations of the Cu and Ir atomic coordinates in the trigonal prisms are much larger than those in the octahedra, and it was necessary to fix the temperature factor of trigonal prismatic Cu to zero to avoid a meaningless negative value. This could indicate the displacement of a proportion of Ir toward the square planes, but this is unlikely to happen to a great extent since the temperature factor of trigonal prismatic Ir is low (0.008(4) Å^2). The introduction of anisotropic temperature factors for Cu and Ir in the trigonal prisms was attempted but the refinement became unstable. It is conceivable that the large size of the trigonal prisms leads to a very disordered distribution of cations within them. For example, if Ir11 was situated at the center of the prismatic site, the distance from each oxide ion would be ~2.4 Å. Therefore, it would be reasonable for Ir to be displaced from the center toward one end of the prism, or to the rectangular faces, or both, forming stronger bonds at the expense of a reduction in coordination number. As may be seen in Figure 4, parts a and b, the Ba/O layers are very distorted, almost to the point of being unrecognizable. There is also less difference in size between the octahedral and trigonal prismatic sites than in the ideal structure, the trigonal prisms occupying little more space parallel to *c* than the octahedra.

The structural refinement of $Ba_{16}Cu_3Ir_{10}O_{39}$ proved to be difficult due to the large number of variables resulting from 54 distinct atomic positions. Due to the necessity of placing soft constraints on the Ba−O and octahedral Ir−O bond distances, the refined Ba and O atomic coordinates will not be exactly at their correct positions. However, any errors are unlikely to be large since the weighting used for the soft constraint system was small. This phase, with a trigonal unit cell of 16 layers, is seemingly at the upper limit of complexity for full structural refinement from powder diffraction data. However, the use of combined ND and XRD data sets has allowed us to distinguish between the candidate structures for $Ba_{16}Cu_3Ir_{10}O_{39}$, model **c** being the correct one. Models **b** and **d** may be discounted due to poorer fits, but there was little to choose between models **a** and **c** after the preliminary stages of the refinements. We have discounted model **a** on the basis of an unstable refinement when direct constraints on the atomic coordinates of Ba and O were relaxed. However, the proportion of atoms in different positions when comparing the latter two structures is small. To derive the ideal model **c** from model **a**, just one oxygen atom of the 20 present is moved to a different position (Figure 6, parts

(9) Neubacher, M.; Müller-Buschbaum, Hk. *Z. Anorg. Allg. Chem.* **1992**, *607*, 124.
(10) Wilkinson, A. P.; Cheetham, A. K.; Kunnman, W.; Kvick, Å. *Eur. J. Solid State Inorg. Chem.* **1991**, *28*, 453.
(11) Tomaszewska, A.; Müller-Buschbaum, Hk. *Z. Anorg. Allg. Chem.* **1992**, *617*, 23.

Table 4. Selected Bond Lengths (Å) for $Ba_{16}Cu_3Ir_{10}O_{39}$ (Model c)

Ir1−Ir1	2.55(5)	Ir5−Cu17	2.94(4) ×3	Ir9−Ir18	3.09(7)	Ir13−Cu19	3.04(10) ×3
Ir1−Ir2	2.75(4)	Ir5−Ir17	2.63(14)	Ir10−Ir11	2.60(3)	Ir13−Ir19	2.54(7)
Ir2−Ir16	2.95(8)	Ir6−Ir7	2.64(4)	Ir10−Cu18	2.93(9) ×3	Ir14−Ir15	2.63(4)
Ir2−Cu16	2.68(11) ×3	Ir6−Cu20	2.89(12) ×3	Ir10−Ir18	2.44(7)	Ir15−Cu20	2.92(12) ×3
Ir3−Ir4	2.62(4)	Ir6−Ir20	3.09(7)	Ir11−Ir12	2.57(4)	Ir15−Ir20	2.52(7)
Ir3−Cu16	2.96(11) ×3	Ir7−Ir8	2.49(4)	Ir12−Cu19	2.80(10) ×3		
Ir3−Ir16	2.53(8)	Ir8−Ir9	2.74(4)	Ir12−Ir19	3.18(7)		
Ir4−Ir5	2.51(4)	Ir9−Cu18	2.77(10) ×3	Ir13−Ir14	2.52(4)		
Ir1−O1	2.03(4) ×3	Ir6−O4	2.12(3) ×3	Ir12−O18	1.95(3) ×3	Ir17−O17	2.70(10) ×3
Ir1−O3	2.02(3) ×3	Ir7−O4	2.04(3) ×3	Ir12−O20	2.11(3) ×3	Ir18−O12	2.83(6) ×3
Ir2−O3	2.21(3) ×3	Ir7−O7	2.01(3) ×3	Ir13−O11	1.94(3) ×3	Ir18−O16	1.93(4) ×3
Ir2−O5	1.85(3) ×3	Ir8−O7	2.05(3) ×3	Ir13−O14	1.97(3) ×3	Ir19−O14	1.89(5) ×3
Ir3−O10	1.99(3) ×3	Ir8−O8	2.03(3) ×3	Ir14−O9	2.03(3) ×3	Ir19−O18	2.49(6) ×3
Ir3−O13	2.08(3) ×3	Ir9−O8	2.17(3) ×3	Ir14−O11	2.12(3) ×3	Ir20−O2	2.30(6) ×3
Ir4−O13	2.04(3) ×3	Ir9−O12	1.84(3) ×3	Ir15−O6	1.94(3) ×3	Ir20−O6	2.15(5) ×3
Ir4−O15	2.04(3) ×3	Ir10−O16	2.08(3) ×3	Ir15−O9	2.08(3) ×3		
Ir5−O15	2.05(3) ×3	Ir10−O19	2.07(3) ×3	Ir16−O5	2.37(6) ×3		
Ir5−O17	2.00(3) ×3	Ir11−O19	2.04(3) ×3	Ir16−O10	2.10(5) ×3		
Ir6−O2	1.96(3) ×3	Ir11−O20	2.03(3) ×3	Ir17−O17	2.31(10) ×3		
Cu16−O5	2.60(11)	Cu17−O17	2.37(3) ×2	Cu18−O16	2.07(7)	Cu20−O2	2.65(11)
Cu16−O5	1.97(9)	Cu17−O17	2.38(3) ×2	Cu19−O14	2.61(11)	Cu20−O2	1.94(10)
Cu16−O5	1.97(9)	Cu18−O12	3.00(12)	Cu19−O14	2.09(8)	Cu20−O2	1.94(10)
Cu16−O10	2.82(11)	Cu18−O12	2.38(7)	Cu19−O14	2.08(8)	Cu20−O6	2.92(11)
Cu16−O10	2.20(9)	Cu18−O12	2.35(8)	Cu19−O18	2.61(11)	Cu20−O6	2.23(10)
Cu16−O10	2.21(9)	Cu18−O16	2.73(12)	Cu19−O18	2.04(8)	Cu20−O6	2.22(10)
Cu17−O17	2.89(13) ×2	Cu18−O16	2.03(8)	Cu19−O18	2.03(8)		
Ba1−O1	2.85(3) ×2	Ba3−O6	3.07(5)	Ba5−O11	2.94(5)	Ba7−O17	3.06(3)
Ba1−O2	3.07(4) ×2	Ba3−O7	2.84(4)	Ba5−O12	3.09(4)	Ba7−O18	2.58(4)
Ba1−O2	3.04(4) ×2	Ba3−O7	2.88(5)	Ba5−O12	3.18(4)	Ba7−O19	2.78(4)
Ba1−O3	3.02(3) ×2	Ba3−O8	2.98(4)	Ba5−O13	2.80(4)	Ba8−O15	2.60(4)
Ba1−O4	2.67(3) ×2	Ba3−O9	2.66(3)	Ba5−O14	3.42(4)	Ba8−O16	3.10(3)
Ba2−O1	2.77(4)	Ba4−O5	2.51(4)	Ba6−O10	3.13(4)	Ba8−O17	2.99(4)
Ba2−O2	2.43(4)	Ba4−O6	3.11(4)	Ba6−O11	2.61(4)	Ba8−O17	3.09(5)
Ba2−O2	3.46(4)	Ba4−O7	2.71(4)	Ba6−O12	2.45(4)	Ba8−O18	2.92(6)
Ba2−O3	2.91(4)	Ba4−O8	2.95(5)	Ba6−O13	2.88(5)	Ba8−O18	2.98(6)
Ba2−O3	2.90(6)	Ba4−O8	2.81(5)	Ba6−O13	2.86(5)	Ba8−O19	2.90(5)
Ba2−O4	2.89(5)	Ba4−O9	2.82(6)	Ba6−O14	3.02(5)	Ba8−O19	2.85(5)
Ba2−O4	2.95(5)	Ba4−O9	2.92(6)	Ba6−O14	3.00(5)	Ba8−O20	3.09(4)
Ba2−O5	3.51(4)	Ba4−O10	2.64(4)	Ba6−O15	2.96(4)	Ba8−O20	2.69(4)
Ba2−O6	2.57(4)	Ba4−O11	3.05(4)	Ba6−O16	2.50(4)	Ba9−O17	2.55(4) ×2
Ba2−O7	2.89(4)	Ba4−O12	3.16(3)	Ba7−O13	2.83(4)	Ba9−O18	3.35(3) ×2
Ba3−O3	2.68(4)	Ba5−O8	2.57(4)	Ba7−O14	2.62(3)	Ba9−O19	2.83(3) ×2
Ba3−O4	3.07(4)	Ba5−O9	2.83(4)	Ba7−O15	2.92(4)	Ba9−O20	2.93(3) ×2
Ba3−O5	3.03(4)	Ba5−O10	2.84(4)	Ba7−O15	2.84(5)	Ba9−O20	2.86(4) ×2
Ba3−O5	2.94(5)	Ba5−O10	2.91(5)	Ba7−O16	2.89(4)		
Ba3−O6	3.06(4)	Ba5−O11	2.84(5)	Ba7−O16	2.88(5)		

a and c), and the occupancy of Cu and Ir cations is reversed on only one pair of sites (that is, 2 sites from 20). It is therefore unsurprising that the refinements of models **a** and **c** gave very similar agreement in the preliminary stages, and it is conceivable that, with a high likelihood of stacking faults in a structure as complex as this one, the bulk material may contain a proportion of each structure. The refined structure of model **c** has some very short Ir−O distances (the shortest being 1.84(3) Å for Ir9−O12). However, the average octahedral Ir−O bond distance is 2.03 Å, typical for Ir^{4+} and the same as that found for $Ba_5CuIr_3O_{12}$. The shortest Ir−O distances of 1.84(3) Å (Ir9−O12) and 1.85(3) Å (Ir2−O5) both occur in the outer octahedra of tetramers, where it is reasonable to expect a displacement of Ir from the center of the octahedron as the spacing between the highly charged Ir^{4+} cations within the tetramers is maximized. The central octahedra in the trimers and tetramers are all quite regular with typical Ir^{4+}−O bond distances. The intrachain Ir−Ir distances cover a wide range, from 2.44(7) Å (Ir10−Ir18) to 3.18(7) Å (Ir12−Ir19), both the shortest and longest distances involving off-center trigonal prismatic Ir. In fashion similar to $Ba_5CuIr_3O_{12}$, there is substantial disorder in the Ir/Cu distribution over the octahedral and trigonal prismatic sites, the Ir occupancy of the outer octahedra of the trimers and tetramers being 77.3(8)%, slightly more ordered than the 71.4(6)% found in our previous XRD study. The manner of occupancy of the trigonal prismatic sites is again rather unclear, the temperature factor of Cu being fixed at zero to avoid a meaningless negative value; there is likely to be a substantial degree of disorder present in the cation positions within trigonal prisms. In similar fashion to $Ba_5CuIr_3O_{12}$, there is considerable breakdown of the Ba/O layers (Figure 7), which are very buckled and distorted.

Several features are common to both phases, including substantial disorder in the Ir/Cu distribution over the octahedral and trigonal prismatic sites, a disordered distribution of cations within the trigonal prismatic sites and some unusually short metal−metal and metal−oxygen bond distances in the polyhedral chains. In both cases the oxide layers are buckled to such an extent that it becomes difficult to recognize their presence. Trigonal prisms in the ideal structures occupy the space of two octahedra parallel to *c*, but as may be seen in Figures 4a and 8a, the "height" (parallel to [001]) of a trigonal prism in the refined structures is not much greater than

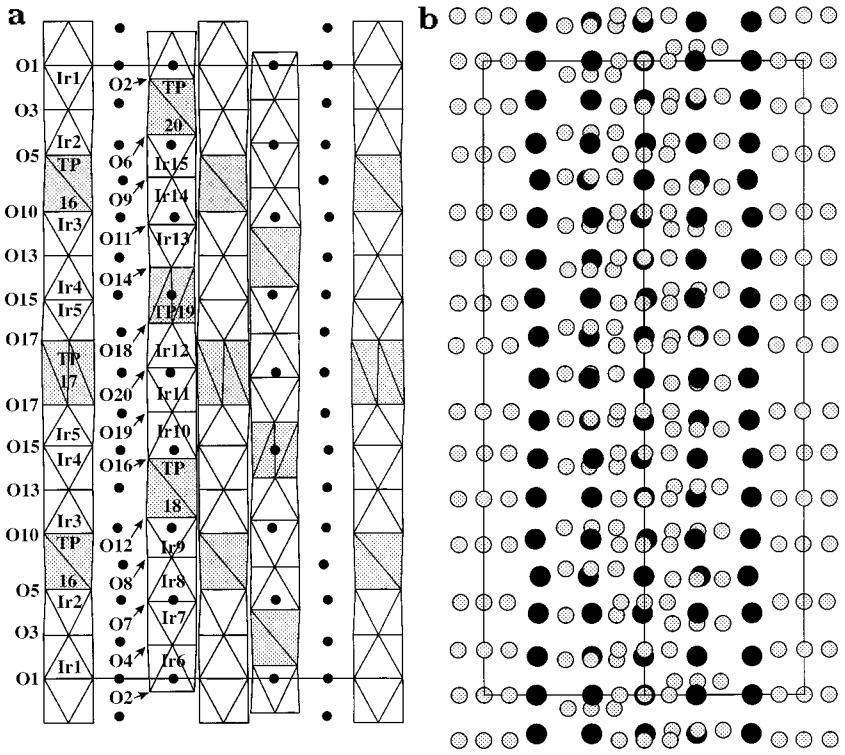

Figure 8. (a) Refined structure of $Ba_{16}Cu_3Ir_{10}O_{39}$ (model **a**) viewed along [110]. Trigonal prisms are shaded, octahedra are unshaded, and black circles represent Ba. Trigonal prisms are numbered after the Ir and Cu atoms they contain. (b) A view of the Ba/O atomic arrangement along [110]. Black circles represent Ba; lightly shaded circles represent O.

that of an octahedron. The distances between cations in the chains therefore show less variation than in the ideal structures, being scattered around an average value which corresponds to c_2 of the composite crystal model. The above discussion describes the average three-dimensional structure of these phases. However, incommensuration and modulation are common features in materials of this type and it is possible that both phases, $Ba_5CuIr_3O_{12}$ and $Ba_{16}Cu_3Ir_{10}O_{39}$, have modulated structures, despite appearing commensurate in ED, XRD, and high-resolution ND data. Indeed, both materials displayed a contrast modulation in their [1$\bar{1}$0] zone lattice images.[1] The structural features giving rise to contrast modulation in the lattice images are unclear but they must occur such that a commensurate repeat unit is obtained over the distance *c*. Our structural refinements do not allow for the presence of a modulation and therefore it is unlikely that the refined structures are entirely accurate, with atomic positions perhaps approximating any modulation as closely as possible. Our inability to model structure modulations may be the cause of the short metal−metal distances within the polyhedral chains and the short Ir−O distances within the octahedra. We note that the ED patterns of these materials, indexed previously[1] in a 3D unit cell, can be reindexed in a 4D unit cell described by the parameters *a*, *b*, c_1, and c_2. For example, the [010] zone ED pattern of $Ba_{16}Cu_3Ir_{10}O_{39}$, indexed in a 4D unit cell, is shown in Figure 9. The use of this strategy reduces the number of unexplained absences among the reflections, and we take this as evidence that our samples actually comprise two substructures which happen to be commensurate. A full and accurate structural determination can only be done using 4D crystallography with a 4D superspace group;[12] we are currently

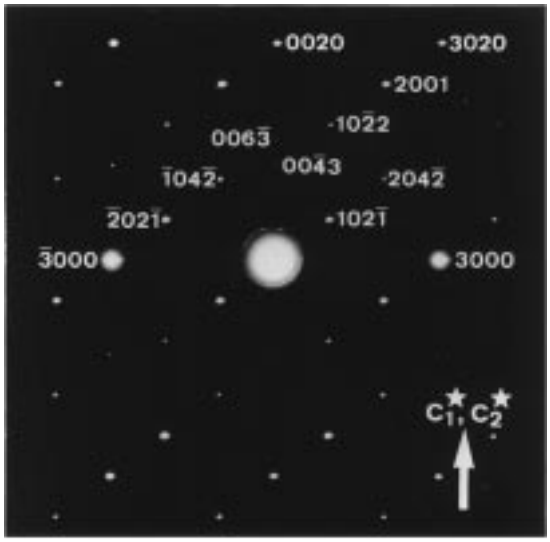

Figure 9. [010] zone electron diffraction pattern of $Ba_{16}Cu_3Ir_{10}O_{39}$, indexed in a 4D unit cell.

undertaking such a study. It will then be possible to give a simpler description of structures such as $Ba_{16}Cu_3Ir_{10}O_{39}$, which are at the upper limit of complexity for full-matrix refinement using the conventional three-dimensional approach.

Acknowledgment. We are grateful to the EPSRC for financial support and to R.M. Ibberson for experimental assistance at the Rutherford-Appleton Laboratory.

CM9807844

(12) Janssen, T.; Janner, A.; Looijenga-Vos, A.; de-Wolff, P. M. *Incommensurate and commensurate modulated structures,* in *International Tables for Crystallography*; Kluwer: Dordrecht, 1995; Vol. C.